

Subcellular Localization and Transport Kinetics of Ruthenium Organometallic Anticancer Compounds in Living Cells: A Dose-Dependent Role for Amino Acid and Iron Transporters

M. Klajner,^{†,§} C. Licon,^{‡,§} L. Fetzner,^{§,||} P. Hebraud,^{†,§} G. Mellitzer,^{‡,§} M. Pfeffer,^{§,||} S. Harlepp,^{*,†,§} and C. Gaidon^{*,‡,§}

[†]UMR7504, I.P.C.M.S., 23 rue du Loess, 67200, Strasbourg, France

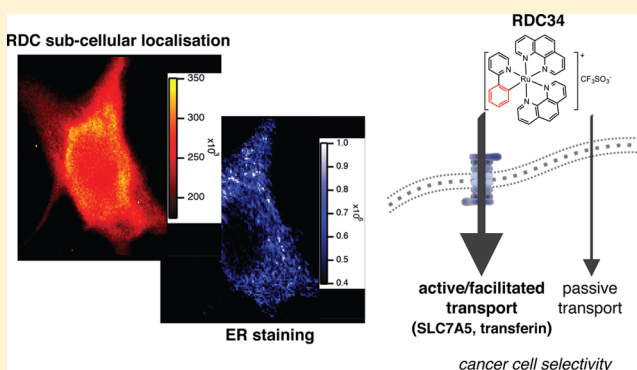
[‡]Molecular Signaling of the Cell Stress Response and Pathology, INSERM 1113, 3 av. Molière, 67200, Strasbourg, France

[§]Université de Strasbourg, Strasbourg, France

^{||}Laboratoire de Synthèses Métallo-Induites, Institut de Chimie, UMR7177, 4 rue Blaise Pascal, Strasbourg, 67000, France

S Supporting Information

ABSTRACT: Ruthenium-based compounds are developed for anticancer treatment, but their mode of action including their import mechanism and subcellular localization remains elusive. Here, we used the intrinsic luminescent properties of cytotoxic organoruthenium (Ru(II)) compounds obtained with an anionic cyclometalated 2-phenylpyridine chelate and neutral aromatic chelating ligands (e.g., phenanthrolines) to follow their behavior in living cells. We established that the difference in sensitivity between cancer cells and noncancerous cells toward one of the compounds correlates with its import kinetics and follows a balance between active and passive transport. The active-transport mechanism involves iron and amino-acid transporters, which are transcriptionally regulated by the drug. We also demonstrated a correlation between the accumulation of these compounds in specific compartments (endoplasmic reticulum, nucleus, mitochondria) and the activation of specific cytotoxic mechanisms such as the mitochondrial stress pathway. Our study pinpoints a novel and complex mechanism of accumulation of ruthenium drugs in cancer cells.



■ INTRODUCTION

In the development and optimization of novel anticancer drugs, several parameters must be taken into account, including the intrinsic cytotoxic activity toward cancer cells and the pharmacokinetics and pharmacodynamics, which altogether are closely linked to the off-target toxicity of the compound toward healthy tissues.¹ These parameters are themselves the consequences of a molecular interaction between the drug and its direct target(s), the drug stability in biological environments, and the water solubility/lipophilicity of the drug. The latter also partly defines the mode of import/export into cells and the accumulation sites of the drug. Fortunate hazard or scientifically-directed adjustments in the balance between these parameters lead to a successful development of a novel anticancer drug.

However, following live import/export mechanisms and the subcellular accumulation sites of a drug often represents a challenge, as the analytical chemistry methods for quantifying the intact drug are not always sensitive enough. Frequently used as an alternative, the modification of the drug with a fluorochrome raises the question about the impact of the

additional ligand on the transport mechanisms, localization, or direct-target interaction.

Few examples of successful chemotherapy are still driving the search for more potent, more selective, less prone to resistance, and better-tolerated drugs. In the past years, a significant interest was given to ruthenium-based drugs, because of the favorable properties of these compounds that make them a suitable basis for the development of antitumor drugs, such as the oxidation state, the ligand-exchange rate and the binding to proteins important for cell survival.^{2,3} Various ruthenium complexes in oxidative state II or III were shown to present ligand-exchange abilities similar to those of platinum complexes, no cross-resistance with cisplatin, and a selective cytotoxicity for cancer cells with a reduced toxicity for healthy tissues, which at least in part can be explained by the selective transportation to cancer cells by the iron-transport system.^{2–13} Two of these compounds, namely NAMI-A and KP1019, have successfully passed initial phase one of clinical trials.^{14,15} Besides these initial successes, the emergence of new

Received: January 31, 2014

Published: May 1, 2014

ruthenium-based therapies has been slowed down by several limitations, such as the relatively poor level of solubility and/or stability these therapies have in aqueous solutions, an unimpressive cytotoxicity (IC_{50} between 10 and 100 μM), and an uncertainty regarding the molecular mechanisms of action responsible for the antitumor effect.

In this respect, the mechanism of action and the direct targets of ruthenium-based drugs are still a matter of debate. Indeed, depending on the drug, several modes of action have been proposed, such as interaction with DNA to activate DNA-damage pathways^{16–20} and inhibition of kinases²¹ or other enzymatic activities,^{22,23} including extracellular metallo-proteases.²⁴ The differences observed may be due to variations in their structure. Even if the ligands attached to the metal are most of the time only weakly bound to ruthenium via a coordination bond, the different nature of the ligands may be sufficient to induce different behaviors for the various complexes studied so far.

To improve the stability of ruthenium complexes and possibly to enhance their cytotoxicity and their pharmacokinetics, we have previously generated several ruthenium-based complexes in which the ligand is bound to the metal (M) via a strong covalent bond such as a C–M σ bond.^{19,25} Besides an increased stability, these compounds present a new variety of ligands, and they differ from each other by their Ru^{II}/Ru^{III} redox factor. We called these molecules ruthenium-derived compounds (RDCs), and we showed previously that several RDCs are cytotoxic for several cisplatin-resistant cancer cell lines.¹⁹ Few of them showed a good antitumor activity both *in vitro* and *in vivo*, with an IC_{50} often between 0.1 and 5 μM , and anticancer property on models of ovarian cancer, melanomas, and gliomas.^{26,27} Importantly, they showed a reduced neurotoxicity in comparison to cisplatin.²⁶ Because we demonstrated previously that cisplatin exerts its neurotoxic effect partly through induction of the p53 pathway,^{28,29} we analyzed the ability of RDCs to interact with DNA and induce p53 proteins. These analyses demonstrated that RDC11 exerts its antitumor effect via DNA-dependent and DNA-independent modes of action.^{26,30,31}

In the present study, we investigate the mode of import and subcellular localization of organoruthenium compounds to gain additional insights about their mode of action. To achieve this, we took advantage of the luminescence of organoruthenium compounds that present aromatic cycles such as RDC34 and RDC44 that we previously characterized for their anticancer properties.²⁷ This intrinsic luminescent property of these anticancer ruthenium-based compounds allowed us to perform these studies using living cells and unmodified compounds. This property rules out the possible problems that would have arisen with molecules to which a fluorochrome had to be attached.

EXPERIMENTAL SECTION

Chemical Compounds. RDC34 and RDC44 were synthesized and purified as previously described.^{32,33} Briefly, the compounds were characterized by ¹H and ¹³C NMR and high-resolution mass spectrometry (HRMS). Organelle-specific fluorescent dyes ER-Tracker Green, MitoTracker Green, Propidium iodide were prepared and used as indicated by the manufacturer (Invitrogen). 2-Deoxy-D-glucose, Oligomycin A, deferoxamine, and D-phenylalanine were purchased (Sigma). Stock solutions of the RDC were 50 mM in dimethyl sulfoxide (DMSO).

Cell Culture. A172 human glioblastoma cells were obtained from the American Type Culture Collection (ATCC). Cells were

manipulated and cultured in Dulbecco's modified Eagle's medium (DMEM) with 10% fetal calf serum (FCS) (Dominique Dutcher) and 1% Penicillin + Streptomycin (Sigma) at 37 °C with 5% CO₂ atmosphere as previously described.³⁴ For live imaging, cells were cultured on coverslips coated with polyornitine (1 $\mu g/mL$) as previously described.³⁵

Primary glia cultures were prepared from 7 d old mouse cerebella using enzymatic and mechanical isolation as previously described.³⁶ Glial cells were separated from neurons by sedimentation and adhesion on uncoated plastic culture plates. After 3 h, unattached neuronal cells were removed by rinsing the plates three times with fresh medium. Attached glial cells were then further cultivated for 5 d before treatment.

Cell Survival. 5000 cells were seeded per well in 96-well microplates (Falcon Multiwell) 48 h prior to any treatment. RDCs were applied for 48 h by diluting the 50 mM DMSO stock solutions in fresh medium (DMEM with 10% serum). 3-(4,5-Dimethylthiazol-2-yl)-2,5-diphenyltetrazolium bromide (MTT) assay was performed as described previously by replacing the medium with fresh medium supplemented with 5 mg/L MTT (Sigma) for 1 h.³⁷ Cells were lysed in isopropanol with 0.04 N HCl. Measurements were performed at 550 nm.

Confocal Microscopy and RDC Accumulation Measurements. A home-built confocal microscope was used. We first visualized the cells before taking any confocal images, to follow a healthy single layer of cells. The typical scan size was around 60 $\mu m \times 60 \mu m$ with a step size of 500 nm. The laser was expended through a telescope and feeds the back focal plane of an objective. The sample was moved with piezoelectric devices. The piezoelectric devices had a total range of approximately 100 μm with a capacitive feedback loop. The repeatability of the system was approximately 20 nm, and the precision was ~ 1 nm. The integration time was adjusted to obtain a good signal-to-noise ratio. The typical integration time was around 50 ms per pixel. The signal was collected through a 50 μm core multimode fiber coupled to a spectrometer splitting the light in the different wavelengths. A charge-coupled device (CCD) camera collected the signal and returned the emission spectrum. This spectrum was then equally divided in 10 subparts. We summed up the intensities in each part and attributed them to an integrated intensity to each average wavelength.

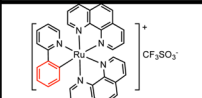
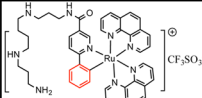
Correlation Factor and Colocalization. We then obtained 10 different images from the same cell at the different wavelengths. Thus, we could compare the fluorescence from the different organelle-specific dyes used, which mostly emitted around 520 nm, and the ruthenium compounds emitting around 750 nm. The images were aligned by x - y translation whose vector was determined by maximizing the correlation between successive images.

$$r = \left(\frac{1}{n-1} \right) \cdot \sum_{x,y} \frac{(f(x,y) - \overline{f(x,y)}) \times (g(x,y) - \overline{g(x,y)})}{\sigma_f \sigma_g}$$

Where r represents the correlation factor, n represents the number of pixels in the image, f was the image obtained from the fluorescent labels, \overline{f} was the average value of that image, g was the image obtained from RDC, \overline{g} the average value of that image, and σ_f , σ_g were the standard deviation of the images.

Import Kinetics. The image acquisition over at least 1 h on the same region and the same cells allowed us to directly compare the fluorescence intensities over time and to link the changes to the intracellular accumulation. We first aligned the images, applying cross-correlation to the stack, and afterward we aligned an X and Y translation to the image to correct the mechanical drift from the time series. This led to a perfect superposition of the images. Then, a region of interest was set such that only the intensity from the cells belonging to the image was taken into account. We summed up the intensity from the region of interest and divided it by the number of pixels involved. The result was an average intensity collected on a cellular area. We obtained from this analysis an intensity versus time array. We used the maximum and minimum intensity values to normalize this

Table 1. Names, Structures, IC₅₀ in A172 Human Glioblastomas, Glial, and Neuronal Cells, and Lipophilicity Index for the Ruthenium-Derived Compounds Used

	Compound	Formula	IC ₅₀ (μM) A172	IC ₅₀ (μM) Glial	IC ₅₀ (μM) Neuron	Lipophilicity LogP(o/w)
N-Ru-C structure	RDC34		0.25 ± 0.23	1.2 ± 0.4	1.15 ± 0.6	2.35 ± 0.04
	RDC44		74 ± 2.6	82 ± 5.3	91 ± 3.6	< 0.5

array. The evolution over time therefore represented the average import kinetics.

Western Blot. Cells were lysed as previously described with a lysis buffer (125 mM tris(hydroxymethyl)aminomethane (Tris)-HCl pH 6.7, NaCl 150 mM, NP40 0.5%, 10% glycerol).³⁸ Proteins were denatured and deposited (75 μg of proteins) on 10% sodium dodecyl sulfate polyacrylamide gel electrophoresis (SDS-PAGE) gel. Western blots were performed using antibodies raised against C/EBP homologous protein (CHOP) (1/1000 dilution, Santa Cruz, CA) or H2AX (S139) (1/2000, Millipore, France) and incubated with the blots overnight. Secondary antibodies (antirabbit, antimouse: Sigma, MA) were incubated at 1:1000 for 2 h. Equal loading of the samples was controlled visualizing actin expression (rabbit anti-β-actin, Sigma, 1:4000).

Quantitative Polymerase Chain Reaction. Cultured cells were lysed with 1 mL of TRIzol per 10 cm² (Invitrogen) to extract RNA according to manufacturer's instructions. RNA samples were ethanol-precipitated twice and 1 μg was used for reverse transcription (High-Capacity cDNA Reverse Transcription Kit, Applied Biosystems). Quantitative polymerase chain reaction (qPCR) was performed using 2 ng/μL cDNA (RNA equivalent) according to manufacturer's instructions (SYBR Green PCR Master Mix, Applied Biosystems) and with 400 μM of each primer (Supporting Information, Table 1). Expression levels were normalized using average of 18S and tri-*n*-butyl phosphate (TBP) (TATAA binding protein) RNA expression.

RESULTS

Ruthenium-Derived Anticancer Compounds Present Fluorescent Properties. We have developed several compounds containing ruthenium in redox state II and bound to aromatic ligands.³³ We previously characterized the cytotoxicity and anticancer activity of RDC34 and RDC44 that both present two phenanthrolines (Table 1).²⁷ RDC44 presents in addition a spermine unit that enforces the water solubility of the compound as indicated by its log p(o/w) using phase-separation experiments³³ (Table 1). RDC34 and RDC44 have an IC₅₀ on cancer cells of 0.25 μM and 74 μM, respectively, in A172 glioblastoma cells that express a wild-type p53 gene. Similar results have been observed on p53-mutated cells (Supporting Information, data #1). Here, we are now showing that the toxicity of the compounds on primary cultures of glial and neuronal cells (noncancerous) was decreased as indicated by an increase of the IC₅₀ (Table 1). Under similar experimental conditions, we obtained an IC₅₀ for cisplatin of 5.4 (±0.8) and 7.9 (±0.6) for A172 and glial cells, respectively. This observation suggested that there is a selectivity of action and/or transport into the cells between cancerous and noncancerous cells for RDC34.

The presence of two phenanthrolines in RDC34 and RDC44 suggested that these compounds could display luminescent properties. Indeed, spectroscopic measurements indicated that

RDC34 and RDC44 when excited at 488 nm exhibited light emission with a pick between 730 and 750 nm (Figure 1A). We have previously shown that related RDCs could intercalate between DNA base pairs.³¹ Therefore, we measured the change in RDC fluorescence upon interaction with DNA. A 4-fold and 10-fold amplification of fluorescence was observed for RDC34 and RDC44, respectively. An increase in fluorescence for RDC34 and RDC44 was also observed when incubated with RNA or bovine serum albumin (BSA) (Figure 1B,C), indicating that these compounds interact *in vitro* as well with RNA and proteins. It is noteworthy that the overall light-emission intensities of RDC44 alone or in interaction with the biological macromolecules were higher compared to RDC34, in particular with BSA.

Subcellular Localization of Organometallic Ruthenium-Containing Compounds in the Endoplasmic Reticulum. The entry and localization of luminescent RDC34 and RDC44 were followed by confocal microscopy on living cells treated for 2 h with the respective drug. Using the same time and measurement parameters, we observed a strong luminescent emission inside the cells caused by RDC34 (Figure 2A) and a much weaker emission for RDC44 (Figure 2B). Interestingly, the emissions for both compounds were markedly perinuclear, suggesting a possible localization in the endoplasmic reticulum (ER). To verify this, we used ER-Tracker Green dye, which is a specific dye for the ER compartment. This marker revealed a good correlation between the localization of the ER-tracker Green dye and the luminescence of RDC34 or RDC44 (Figure 2C,D). We further confirmed the physical and functional relationship between RDC34 and ER by showing that RDC34 strongly increased in a dose-dependent manner the protein level of the ER stress response transcription factor CHOP (Figure 2E) and the mRNA level of CHAC1, a known target gene (Figure 2F). Interestingly, in the same conditions RDC44 did not affect significantly CHOP protein levels or CHAC1 expression, which could be explained by a poor ability of RDC44 to enter cells (Figure 2B) under these conditions. Indeed, cytotoxic concentration of RDC44 (250 μM) also led to the induction of CHAC1 expression (Supporting Information, data #2).

Taken together, this set of experiments indicated that RDC34, which displays normally a weaker emission intensity *in vitro* than RDC44 (Figure 1), accumulates more efficiently in cells compared to RDC44, this being evidenced by its stronger luminescent emission; moreover, it has a physical and functional relationship with the ER.

Subcellular Localization of RDC in the Nucleus and the Mitochondria. To further investigate the subcellular

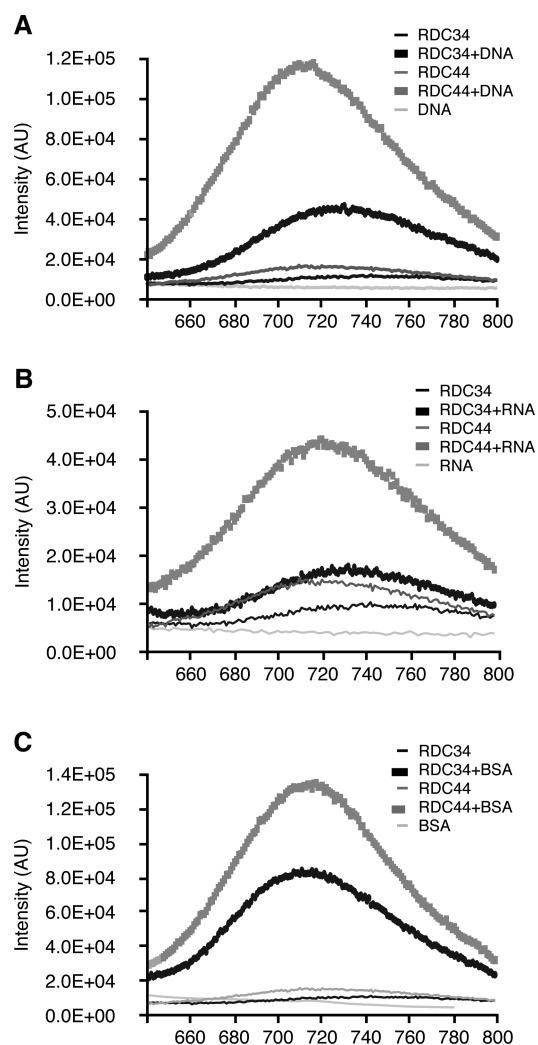


Figure 1. Emission spectra (nm) obtained from RDC34 and RDC44 in interaction with different biopolymers added in large excess compared to RDC molecules. The excitation is set at 488 nm. (A) Lines indicate emission spectra (AU; arbitrary unit) for RDC components (50 μM) alone in aqueous solution, in combination with DNA (sheared salmon sperm DNA, 300 μM), or DNA alone. (B) Lines indicate emission spectra for RDC components (50 μM) alone in aqueous solution, in combination with 16sRNA (60 μM), or 16sRNA alone. (C) Lines indicate emission spectra for RDC components (50 μM) alone in aqueous solution, in combination with BSA (50 μM), or BSA alone.

localization of RDC34, we performed colocalization experiments with dyes specific for the nucleus (propidium iodide) and the mitochondria (MitoTracker Green). We observed that part of the RDC34 was localized inside the nucleus as shown in Figure 3A,B. To independently assess the effect of RDC34 and RDC44 on the nucleus, we showed that RDC34 and to a lesser extent RDC44 induced a DNA damage response as indicated by the phosphorylation of histone H2AX (Figure 3E).

The colocalization studies using the MitoTracker Green (Figure 3D) also revealed that some RDC34 molecules may be localized in the mitochondria (Figure 3C,D). Because of the small size and the dispersion of the mitochondria within the cell a precise colocalization was difficult to assess, but calculation indicated a correlation factor of 0.45 suggesting a good colocalization of RDC34 fluorescence with the MitoTracker Green. As mitochondria develop also a stress response upon

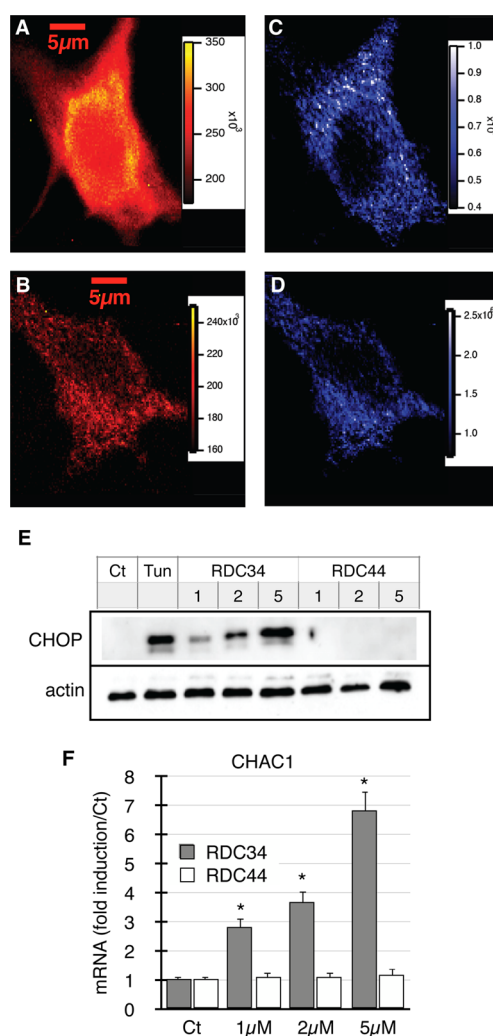


Figure 2. Accumulation of RDC in endoplasmic reticulum and induction of the unfolded protein stress response. A172 cells were incubated for 2 h with RDC34 (A, C) or RDC44 (B, D) at 5 μM , corresponding to the accumulation plateau as indicated by the fluorescence intensity assessed by confocal microscopy. Fluorescence images of RDC34 (A) and RDC44 (B) in A172 cells. Staining of the endoplasmic reticulum was performed using the ER-Tracker Green (C, D). (E) Western blot analysis of cells treated for 24 h at the indicated concentrations (in μM). Tunicamycin (Tun) was used at 5 $\mu\text{g}/\text{mL}$. Immunoblotting was performed with antiactin and anti-CHOP antibodies. Data are representative of three independent experiments. Ct stands for cells treated without the drugs. (F) Cells were treated with RDC34 or RDC44 at the indicated concentration (in μM) for 24 h. Reverse transcription (RT) qPCR was performed using primers for CHAC1. Data are represented as mean (\pm standard deviation) of fold inductions relative to untreated cells (Ct) and were normalized with both 18s and TBP levels. Asterisks indicate statistically significant difference ($p < 0.01$) compared to control, as calculated by a one-way ANOVA test followed by a Tukey test.

damages, we analyzed the activation of SATB1/2 proteins and their target gene HSP60, which are markers of this stress response.³⁹ Interestingly, cells treated with RDC34 showed an induction of both SATB2 and HSP60 expressions (Figure 3F).

Altogether these studies indicated that RDC34 was localized in at least three intracellular compartments, ER, mitochondria, and nucleus. Their localization into these compartments also correlated with the activation of specific stress-response mechanisms, such as CHOP, H2AX, or SATB2.

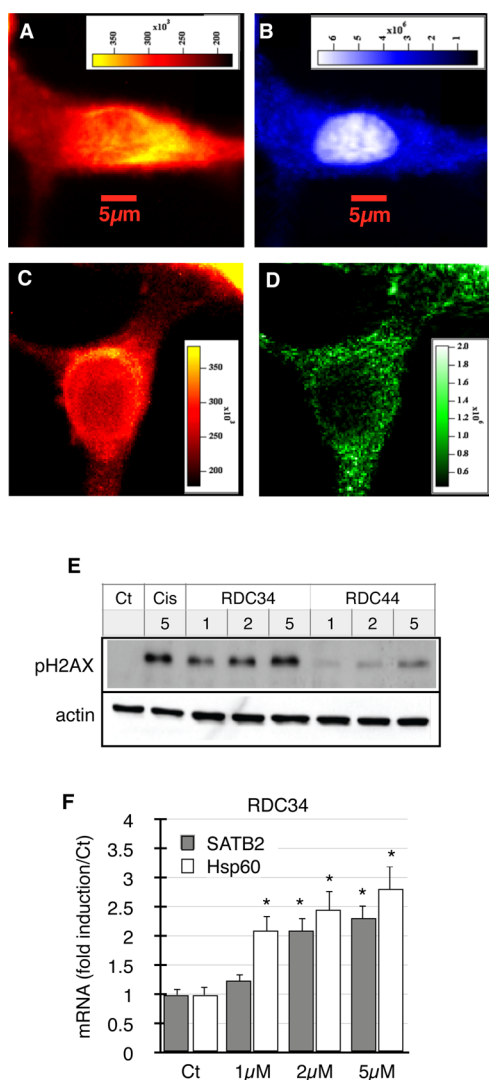


Figure 3. Accumulation of RDC in the nucleus and the mitochondria, and induction of DNA damage and mitochondrial stress response. (A, B, C, D) A172 cells were incubated for 2 h with RDC34 ($5 \mu\text{M}$) to the accumulation plateau as indicated by the fluorescence intensity assessed by confocal microscopy. (B, D) Staining of the nucleus or the mitochondria was performed using the propidium iodide (B) and MitoTracker Green (D), respectively. (E) Western blot analysis of cells treated for 24 h at the indicated concentrations. Immunoblotting was performed with antiactin and anti-H2AX(S139) antibodies. Cisplatin (Cis; $5 \mu\text{M}$) was used as positive control. Data are representative of three independent experiments. (F) Cells were treated with RDC34 at the indicated concentrations for 24 h. RT-qPCR was performed using primers for SATB2 and HSP60. Data are represented as mean (\pm standard deviation) of fold inductions relative to untreated cells (Ct) and were normalized with both 18s and TBP levels. Asterisks indicate statistically significant difference ($p < 0.01$) compared to control, as calculated by a one-way ANOVA test followed by a Tukey test.

Kinetics of Import in Cancerous and Noncancerous Cells. After determination of the intracellular localization, we focused on RDC34 intracellular accumulation over time. For this, we grew cells on polyornitine-treated coverslips, and after replacing culture medium with a RDC34 containing medium we performed time-lapse imaging as shown in Figure 4A. For appropriate comparative evaluation, the same image setup parameters were conserved for all pictures, permitting the direct

linking of the intensity evolution to the accumulation. As specified in the Experimental Section, to further analyze the kinetics, we extracted the average intensity from the selected cells and normalized the maximum values obtained at 200 min or at the plateau in the time-lapse analysis with the number of pixels involved to attribute an intensity evolution value between 0 and 1 (Figure 4B,C,D). We observed in all the different tested cells that the curves obtained at $5 \mu\text{M}$ did not superimpose onto the ones obtained at $10 \mu\text{M}$.

If we hypothesize the extracellular solution to be a reservoir of ruthenium compounds and the collected intensity to be the average concentration on the cellular volume, the second Fick's law tells us that the only parameter that influences the kinetics and the maximal intracellular concentration is the initial reservoir concentration. Thus, dividing our time series by the value reached at saturation directly shows whether the kinetics are purely diffusive or not. The fact that the curves do not superimpose therefore means that the kinetics differ from diffusion. Next, we assumed the simplest case where the kinetics are first-order in RDC concentration; in this case an exponential increase of the intensity would be observed, with a characteristic time independent of the initial concentration. Although our observed intensity versus time relationship may be well-described by a single exponential function, the deduced kinetic rate did depend on the initial RDC concentration (Figure 4B). Consequently, a purely passive diffusion mechanism can be excluded, thus suggesting that either facilitated or active transport must take part in the entrance mechanisms of RDC. We then followed the uptake of these drugs in healthy cells as shown in Figure 4C,D. Interestingly, the rate of drug intake at $5 \mu\text{M}$ was reduced in glial and neuronal cells compared to A172. In addition, we observed no superposition when the only changing parameter was the concentration, as observed in A172 cells. The adjustment was an exponential as described in A172 cells. Surprisingly, when the extracellular concentration was raised to $10 \mu\text{M}$ the rate of import was higher in healthy cells compared to A172 cells.

Altogether, the kinetic analysis suggested that the import might involve multiple kinds of mechanisms including facilitated and active processes. In addition, the rate of import is dependent on the extracellular concentration of the drug and the cell type.

RDC34 Multiple Intracellular Import Mechanisms Including Amino Acid Transporters. To better understand the mechanisms of RDC34 cellular import, we tested inhibitors of adenosine 5'-triphosphate (ATP) production to discriminate between passive and active mechanisms. We treated cells with oligomycin and 2-deoxy-D-glucose, classically used to inhibit ATP production, to block active import mechanisms.⁴⁰ As shown in Figure 5A the percentage of active-import mechanism involved in RDC34 accumulation increased when the concentration of RDC34 applied to the cells was lower than $5 \mu\text{M}$. At $1 \mu\text{M}$, 50% of the import is mediated by a mechanism dependent upon ATP production.

To further characterize the import mechanisms for RDC34 we focused on the ferritin/transferrin receptor system.⁴¹ Several publications have documented an interaction between ruthenium compounds and transferrin.⁴² The interaction is supposed to be based on the fact that ruthenium belongs to the family of iron. Interestingly, we observed that RDC34 increased the expression of ferritin, which is an iron intracellular packaging component, and decreased the expression of the transferrin receptor (TFRC), indicating that RDC34 regulates

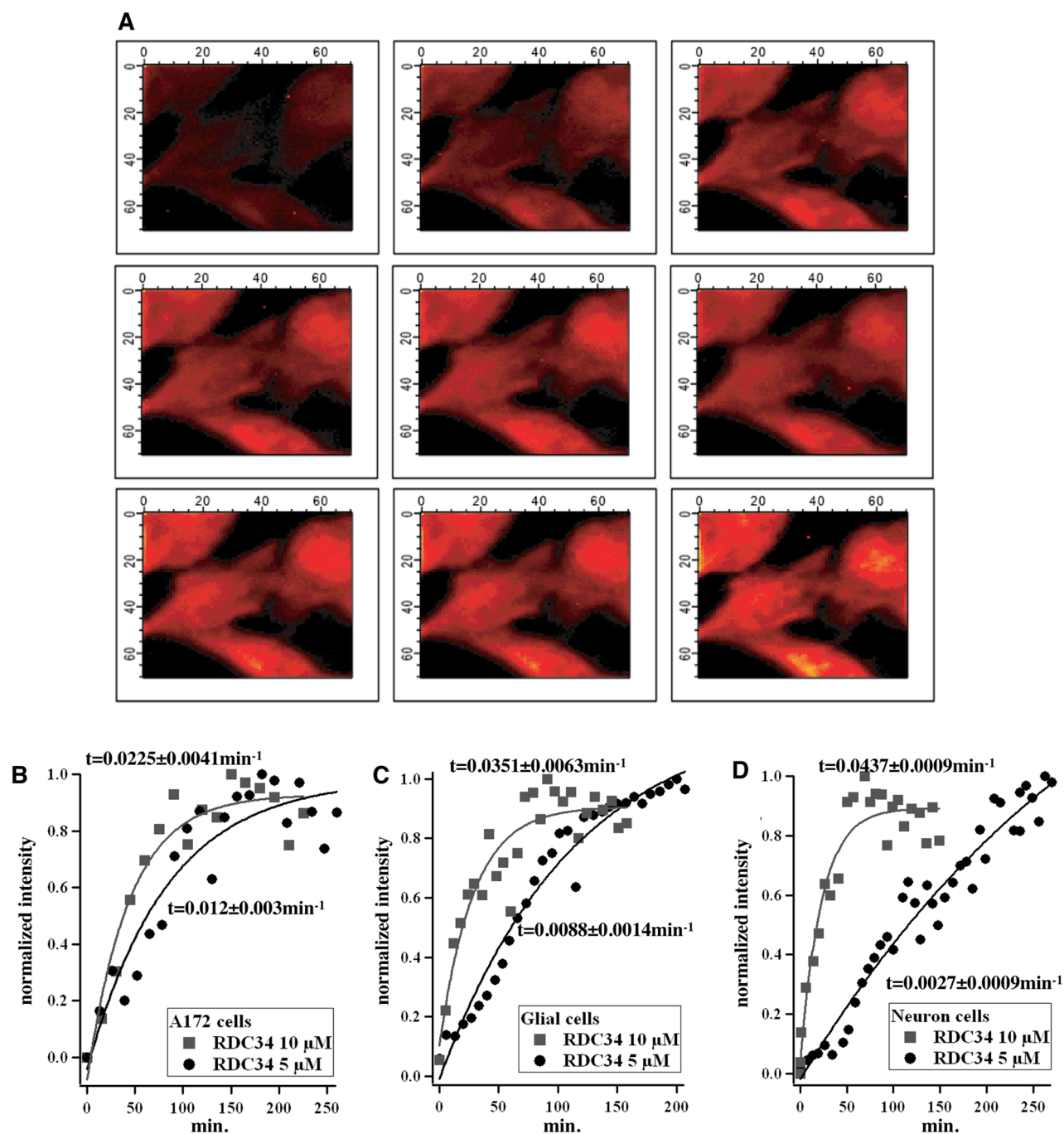


Figure 4. RDC intracellular accumulation observed with confocal microscopy over time. (A) Raw-image time series (left to bottom right) from A172 cells treated with 5 μM RDC34. The delay time between two consecutive images is around 8 min. The intensity range is fixed for all images to highlight the evolution. (B, C, D) The normalized accumulative intensity (1 being the maximal intensity measured) over time for RDC34 at 5 μM and 10 μM and the exponential adjustments in A172 (B), glial (C), and neuronal (D) cells.

like iron the expression of ferritin and TFRC, thus suggesting that the cells might consider RDC34 as iron (Figure 5B). Therefore, we tested how deferoxamine, which is known to chelate iron, might affect RDC import (Figure 5C). We observed that deferoxamine increased by approximately 25% the accumulation of RDC34 inside the cells. This result indicated that chelation of iron from the medium, and therefore leaving more iron transporter available, favored the import of RDC34. It also suggested that deferoxamine did not chelate RDC34.

Additional RT-qPCR analyses of various cellular transporters showed that RDC34 induced the expression of the amino acid transporter SLC7A5 (Figure 5B).⁴³ Amino acid transporters have been described to import also several chemical compounds including drugs. Therefore, we hypothesized that SLC7A5 could provide a means of cellular entry for RDC34. To verify this, we used D-phenylalanine that was previously shown to inhibit SLC7A5-dependent import.⁴⁴ Preincubation of cancer cells with D-phenylalanine reduced the accumulation of RDC34 (Figure 5D), suggesting that SLC7A5 participates in the cellular import of RDC34.

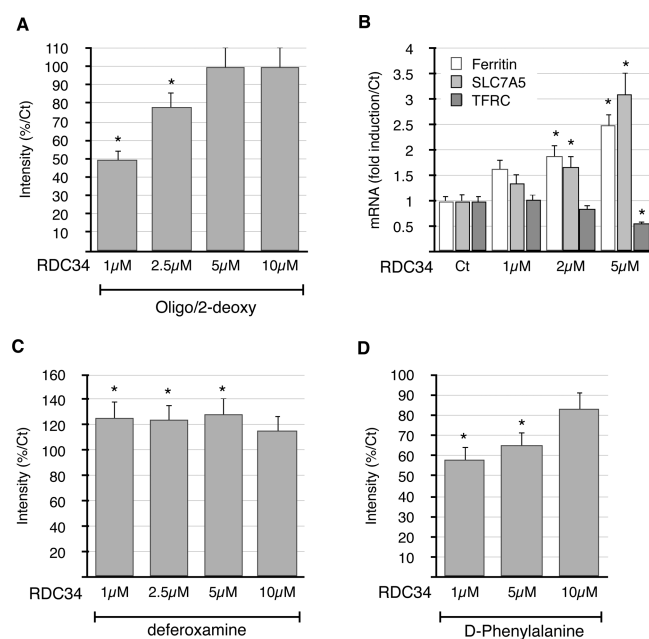


Figure 5. Importance of iron and amino acid transport in RDC intracellular import. (A) Active transport mechanisms were inhibited in A172 cells by using oligomycin ($5 \mu\text{M}$) and 2-deoxy-glucose (50 mM) preincubated for 1 h before adding RDC34 at the indicated concentration for 2 h. Accumulation of RDC34 was measured by fluorescence intensity using confocal microscopy at the end of the incubation time. Bars indicate mean (\pm standard deviation) of intensity. (B) Cells were treated with RDC34 at the indicated concentrations for 24 h. RT-qPCR was performed using primers for Ferritin, SLC7A5, and the transferrin receptor (TFRC). Data are represented as mean (\pm standard deviation) of fold inductions relative to untreated cells (Ct) and were normalized with both 18s and TBP levels. (C, D) A172 cells were preincubated with deferoxamine ($100 \mu\text{M}$) and D-phenylalanine (1 mM) for 1 h before adding RDC34 at the indicated concentration for 2 h. Accumulation of RDC34 was measured by fluorescence intensity using confocal microscopy at the end of the incubation time. Bars indicate mean (\pm standard deviation) of intensity. Asterisks indicate statistically significant difference ($p < 0.01$) compared to control, as calculated by a one-way ANOVA test followed by a Tukey test.

DISCUSSION

Metal-based compounds are intensively investigated as anticancer drugs due to their physicochemical properties such as their redox potential, ligand-exchange rate, the possibility of attaching more than four ligands to them, and others. Unfortunately, up to now the persistent lack of precise biochemical and biological characterizations retard their optimization and development toward clinical practice. In this regard, the ability of a specific compound to exert its biological function is dependent on multiple factors, such as its affinity to its intracellular targets, its intrinsic biochemical properties that might affect the function of its intracellular targets, and its ability to enter and be localized in specific compartments of the cell. Previously, studies were performed on this aspect with metal-based compounds, such as the anticancer compounds Nami-A or KP1019,⁴⁵ or DNA intercalators such as dipyridophenazine (dppz) complexes of Ru(II).^{40,46,47} These compounds have the specificity of presenting nitrogen–metal coordination bonds, and in the case of Nami-A and KP1019, they display relatively low toxicities on cancer cells ($\text{IC}_{50} > 10 \mu\text{M}$).³⁰ In this study, we investigated for the first time the

subcellular localization and the import processes of organometallic ruthenium compounds (that contained ruthenium “Ru–C” bond) showing strong cytotoxic properties.

Aromatic Ligands As a Tool to Follow Metal-Based Import/Export and Interaction with Biological Macromolecule. Following the outcome of a defined biologically active compound in cells in terms of import and subcellular localization is often a difficult task, being limited by available technological tools. For instance, it remains challenging to address these questions with metal-based anticancer compounds due to the limitations of the chemical analyses to locate these compounds in living cells. It often requires the use of cellular invasive methods or important chemical modifications. One of these modifications is the addition of a fluorescent moiety to the molecule. If this addition permits following the molecule *in cellulo* using microscopy, it also significantly modifies the molecule structure, which might bring artifacts in term of uptake, localization, and interaction with intracellular components. An alternative is to use induced coupled plasma mass spectrometry (ICP-MS) to quantify the presence of the metal in specific location after subcellular compartment isolation. This approach has two limits; the first is that ICP-MS quantifies only the metal and does not guarantee that the molecule is intact, and the second is that cellular manipulation to isolate the subcellular compartments can also alter the distribution of the compound. In our pursuit of developing highly cytotoxic anticancer compounds based on ruthenium, we designed and characterized an organometallic ruthenium compound, called RDC34, that presents Ru(II) cyclometalated to a phenylpyridine ligand via a covalent C–Ru bond that is further stabilized by an intramolecular N–Ru coordination bond. In addition, this compound presents two phenanthrolines as chelating ligands. This compound is highly cytotoxic toward cancer cells ($\text{IC}_{50} < 1 \mu\text{M}$) and reduces *in vivo* tumor growth (Table 1 and refs 27 and 33). Interestingly, the presence of the two phenanthrolines provides a fluorescence property that is amplified when RDC34 interacts with biological macromolecules such as DNA, RNA, and proteins (Figure 1). The exact biological significance of these nonselective interactions with DNA, RNA, and BSA remains to be established, as the experiments were done in tubes with purified molecules. In this respect, a confirmation of this lack of selectivity in cells would help to explain why these compounds act on several signaling pathways (CHOP/CHAC1; H2AX; SATB2/HSP60). Although RDC34 multiple mode of action might be regarded as a reason for its low selectivity, it may help to circumvent some resistance mechanisms and provide a compound being active on a very heterogeneous population of cancer cells in the tumor. The fluorescence intensity of RDC34 increases by approximately 3-fold in the presence of DNA, RNA, and BSA. Similar observations were done with an RDC34 variant that presents a spermine tail that increases its water solubility (Figure 1). Removal of a single phenanthroline, such as in the compound RDC11,²⁶ abrogates the fluorescence property (data not shown). Interestingly, addition of other aromatic ligands, such as in RDC56, also provides an interesting fluorescence property (Supporting Information, data #3). Therefore, derivatives of organoruthenium compounds with aromatic ligands, like RDC34 and RDC56, represent unique anticancer metal-based compounds that can be studied to gain a better understanding of the subcellular localization and import/export mechanisms of this class of novel therapeutic drugs, providing

information necessary for their further development and improvement of their reactivity.

Intracellular Localization of the Ruthenium Compounds. Using dyes that present subcellular selective localization, we observed accumulation of RDC34 in the nucleus, the endoplasmic reticulum, and the mitochondria of cancer cells (Figure 2, 3). Previously, accumulation of the ruthenium-based anticancer drugs Nami-A and KP1019 was observed in the nucleus and the mitochondria.⁴⁵ Here we also see an accumulation of RDC34 in the perinuclear part of the cell that corresponds in part to the endoplasmic reticulum. It remains to be established whether it is specific to the family of compounds with a cyclometalated phenylpyridine structure like those in RDC34 and RDC11. In addition, we are showing here that the presence of RDC34 in these compartments has specific functional consequences such as the induction of compartment-specific stress-response pathways like the induction of H2AX phosphorylation and CHOP/UPR and SATB2 expression (Figures 2 and 3). These molecular mechanisms can account for the cytotoxic or cytostatic activity of RDC34 on cancer cells.

Influence of the Lipophilicity on the Import of Ruthenium Compounds. The compound RDC44 has been developed to improve the water solubility of RDC34 by adding a spermine tail, which, however, drastically reduced its cytotoxicity (Table 1).²⁷ Interestingly, the ability of RDC44 to interact and increase its fluorescence upon interaction with DNA, RNA, or BSA does not seem to be affected: the fluorescence is improved with RDC44 *in vitro* when it interacts with biological macromolecules, in particular with BSA (Figure 1). However, the fluorescence emitted by RDC44 in cancer cells is reduced compared to that of RDC34. This observation suggests that RDC44 tends to accumulate less in cells. Although some RDC44 accumulates in cells anyway, we did not observe cytotoxicity or significant induction of stress-response pathways, such as H2AX phosphorylation or CHOP induction. It appears therefore that the lipophilicity status of the compound might impact partly the ability of the compound to enter the cells under these conditions. Additional experiments using variants of RDC34 might be necessary to assess whether there is a strict correlation between the lipophilicity and the accumulation in cancer cells.

Mode of Import of the Ruthenium Compounds. Experiments were performed with drugs that block or reduce selected cellular import mechanisms. The results obtained suggest that several import mechanisms participate in the active or facilitated entry of RDC34 in cancer cells. More specifically, we observed a contribution of active-transport mechanisms and amino acids transporters (Figure 5). The active import of ruthenium-based compounds was previously described for dipyrido[3,2-a:2',3'-c]phenazine (dppz) DNA intercalators.⁴⁰ In this study, we now demonstrate that it is also the case for smaller organometallic compounds, and in addition we show that the contribution of these transport mechanisms is drug- and concentration-dependent. The lower the concentration of the compound, the higher the contribution of the active-import mechanism. This suggests that the concentration gradient at high concentration enforces the passive transport. We also observed that the use of the iron chelation drug deferoxamine improved the accumulation of RDC34, suggesting that RDC34 import might involve iron transport mechanisms such as ferritin and the transferrin receptor. This feature is supported by several observations. First, the normalized accumulation curves

over time present concentration dependence. The dependence proves that the import is not purely diffusive, and some active transporter might be implicated (Figure 4). Second, RDC34 induces, like iron, the expression of transferrin and amino acid transporter such as SLCA7A5 (Figure 5).⁴¹

Selectivity between Cancer Cells and Noncancer Cells. RDC34 shows some selectivity toward glial cancer cells versus healthy glial cells, with IC_{50} values of $0.25 \mu\text{M}$ and $1.2 \mu\text{M}$, respectively (Table 1). We already observed such selectivity with RDC11, a ruthenium compound with the cyclometalated phenylpyridine, one phenanthroline, and two acetonitriles. However, this selectivity is not observed with RDC44 that has an additional spermine tail compared to RDC34.²⁶ The import studies that we performed indicated that the import kinetics differed between cancer and normal cells. The import kinetics were much higher for cancer cells compared to normal cells (neurons or glial cells) (Figure 4). Interestingly, at $10 \mu\text{M}$ RDC34 the kinetics was drastically increased in all cells but even more in normal cells. These results indicated that in terms of import, cancer cells have a higher transport potential at low concentration of the drug than the healthy cells, which might be due to a constitutive high number of receptors/channels required for importing components necessary for cancer cell growth or due to a higher adaptability (induction of these receptors/channels upon treatment). This leads to selectivity between cancer cells and healthy cells, but this selectivity tends to decrease with an increasing drug concentration. Such concentration dependence could be explained by the fact that the active-import mechanisms are more important at low concentration (see above and Figure 5).

Altogether our data suggest a model in which RDC34 at low concentration enters into cancer cells more easily than it enters into normal cells through active mechanisms that are induced by RDC34 at the transcriptional level. However, at higher concentrations, this selectivity is lost due to the concentration gradient pressure (Figure 6). The distribution of RDC34 in the

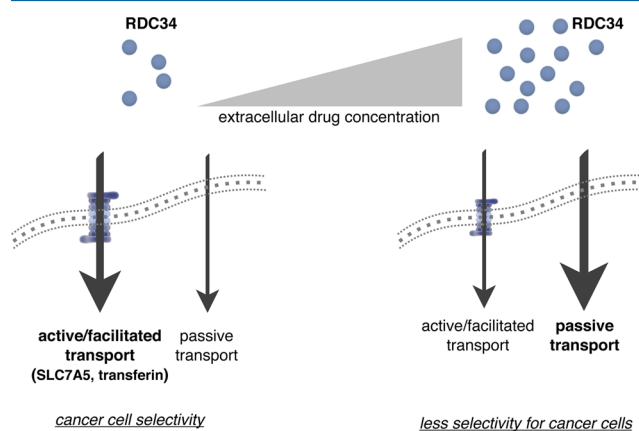


Figure 6. Scheme of the import mechanism representing proportion of active transport as a function of extracellular organoruthenium compound concentration.

cells is complex and reflects the diversity of the signaling pathways that are induced by RDC34. In particular, not only nuclear and ER stress mechanisms are activated, but also a mitochondrial stress response. Hence, our findings provide novel and critical information on the possibly induced

molecular mechanisms and on the potential direct targets of organoruthenium anticancer drugs.

■ ASSOCIATED CONTENT

● Supporting Information

Graph of cytotoxic response, histogram of fold inductions, table of genetic data, and RDC56 IC₅₀ values. This material is available free of charge via the Internet at <http://pubs.acs.org>.

■ AUTHOR INFORMATION

Corresponding Authors

*E-mail: gaiddon@unistra.fr. (C.G.)

*E-mail: harlepp@ipcms.u-strasbg.fr. (S.H.)

Notes

The authors declare no competing financial interest.

■ ACKNOWLEDGMENTS

This work was supported by CNRS (C.G.), Association pour la Recherche Contre le Cancer (Grant 3288), La Ligue Contre le Cancer, Institut National du Cancer, and CONECTUS Alsace, European COST CM1105, CONACYT, the Laboratory of Excellence (LABEX) "Chemistry of Complex Systems" Univ. of Strasbourg and the FRC "synergie" (Univ. of Strasbourg). We are also thankful to P. Wlosik and L. Mathern for their technical and administrative support.

■ REFERENCES

- (1) Doherty, M. M.; Michael, M. *Curr. Drug Metab.* **2003**, *4*, 131–49.
- (2) Bruijninx, P. C.; Sadler, P. J. *Curr. Opin. Chem. Biol.* **2008**, *12*, 197–206.
- (3) Jakupec, M. A.; Galanski, M.; Arion, V. B.; Hartinger, C. G.; Keppler, B. K. *Dalton Trans.* **2008**, 183–94.
- (4) Markman, M. *Expert Opin. Drug Saf.* **2003**, *2*, 597–607.
- (5) Kelland, L. *Nat. Rev. Cancer* **2007**, *7*, 573–84.
- (6) Allardyce, C. S.; Dyson, P. J. *Platinum Met. Rev.* **2001**, *45*, 62.
- (7) Dyson, P. J.; Sava, G. *Dalton Trans.* **2006**, 1929–33.
- (8) Giraldi, T.; Sava, G.; Bertoli, G.; Mestroni, G.; Zassinovich, G. *Cancer Res.* **1977**, *37*, 2662–6.
- (9) Keppler, B. K.; Balzer, W.; Seifried, V. *Arzneim. Forsch.* **1987**, *37*, 770–1.
- (10) Sava, G.; Pacor, S.; Zorzet, S.; Alessio, E.; Mestroni, G. *Pharmacol. Res.* **1989**, *21*, 617–28.
- (11) Fruhauf, S.; Zeller, W. J. *Cancer Res.* **1991**, *51*, 2943–8.
- (12) Morris, R. E.; Aird, R. E.; Murdoch Pdel, S.; Chen, H.; Cummings, J.; Hughes, N. D.; Parsons, S.; Parkin, A.; Boyd, G.; Jodrell, D. I.; Sadler, P. J. *J. Med. Chem.* **2001**, *44*, 3616–21.
- (13) Scolaro, C.; Bergamo, A.; Brescacin, L.; Delfino, R.; Cocchiello, M.; Laurenczy, G.; Geldbach, T. J.; Sava, G.; Dyson, P. J. *J. Med. Chem.* **2005**, *48*, 4161–71.
- (14) Hartinger, C. G.; Zorbas-Seifried, S.; Jakupec, M. A.; Kynast, B.; Zorbas, H.; Keppler, B. K. *J. Inorg. Biochem.* **2006**, *100*, 891–904.
- (15) Rademaker-Lakhai, J. M.; van den Bongard, D.; Pluim, D.; Beijnen, J. H.; Schellens, J. H. *Clin. Cancer Res.* **2004**, *10*, 3717–27.
- (16) Mei, H. Y.; Barton, J. K. *Proc. Natl. Acad. Sci. U.S.A.* **1988**, *85*, 1339–43.
- (17) Brabec, V. *Prog. Nucleic Acid Res. Mol. Biol.* **2002**, *71*, 1–68.
- (18) Zeglis, B. M.; Pierre, V. C.; Barton, J. K. *Chem. Commun. (Cambridge, U.K.)* **2007**, 4565–79.
- (19) Gaiddon, C.; Jeannequin, P.; Bischoff, P.; Pfeffer, M.; Sirlin, C.; Loeffler, J. P. *J. Pharmacol. Exp. Ther.* **2005**, *315*, 1403–11.
- (20) Hayward, R. L.; Schornagel, Q. C.; Tente, R.; Macpherson, J. S.; Aird, R. E.; Guichard, S.; Habtemariam, A.; Sadler, P.; Jodrell, D. I. *Cancer Chemother. Pharmacol.* **2005**, *55*, 577–83.
- (21) Smalley, K. S.; Contractor, R.; Haass, N. K.; Kulp, A. N.; Atilla-Gokcumen, G. E.; Williams, D. S.; Bregman, H.; Flaherty, K. T.; Soengas, M. S.; Meggersq, E.; Herlyn, M. *Cancer Res.* **2007**, *67*, 209–17.
- (22) Ang, W. H.; De Luca, A.; Chapuis-Bernasconi, C.; Juillerat-Jeanneret, L.; Lo Bello, M.; Dyson, P. J. *ChemMedChem.* **2007**, *2*, 1799–1806.
- (23) Dougan, S. J.; Habtemariam, A.; McHale, S. E.; Parsons, S.; Sadler, P. J. *Proc. Natl. Acad. Sci. U.S.A.* **2008**, *105*, 11628–33.
- (24) Gava, B.; Zorzet, S.; Spessotto, P.; Cocchiello, M.; Sava, G. *J. Pharmacol. Exp. Ther.* **2006**, *317*, 284–91.
- (25) Leyva, L.; Sirlin, C.; Rubio, L.; Franco, C.; Le Lagadec, R.; Spencer, J.; Bischoff, P.; Gaiddon, C.; Loeffler, J. P.; Pfeffer, M. *Eur. J. Inorg. Chem.* **2007**, 3055–3066.
- (26) Meng, X.; Leyva, M. L.; Jenny, M.; Gross, I.; Benosman, S.; Fricker, B.; Harlepp, S.; Hebraud, P.; Boos, A.; Wlosik, P.; Bischoff, P.; Sirlin, C.; Pfeffer, M.; Loeffler, J. P.; Gaiddon, C. *Cancer Res.* **2009**, *69*, 5458–5466.
- (27) Vidimar, V.; Meng, X.; Klajner, M.; Licon, C.; Fetzer, L.; Harlepp, S.; Hebraud, P.; Sidhoum, M.; Sirlin, C.; Loeffler, J. P.; Mellitzer, G.; Sava, G.; Pfeffer, M.; Gaiddon, C. *Biochem. Pharmacol.* **2012**, *84*, 1428–36.
- (28) Benosman, S.; Gross, I.; Clarke, N.; Jochemsen, A. G.; Okamoto, K.; Loeffler, J. P.; Gaiddon, C. *Cell Death Differ.* **2007**, *14*, 2047–2057.
- (29) Benosman, S.; Meng, X.; Von Grabowiecki, Y.; Palamiuc, L.; Hritcu, L.; Gross, I.; Mellitzer, G.; Taya, Y.; Loeffler, J. P.; Gaiddon, C. *J. Biol. Chem.* **2011**, *286*, 43013–25.
- (30) Bergamo, A.; Gaiddon, C.; Schellens, J. H.; Beijnen, J. H.; Sava, G. *J. Inorg. Biochem.* **2012**, *106*, 90–9.
- (31) Klajner, M.; Hebraud, P.; Sirlin, C.; Gaiddon, C.; Harlepp, S. *J. Phys. Chem. B* **2010**, *114*, 14041–7.
- (32) Boff, B.; Gaiddon, C.; Pfeffer, M. *Inorg. Chem.* **2013**, *52*, 2705–15.
- (33) Fetzer, L.; Boff, B.; Ali, M.; Xiangjun, M.; Collin, J. P.; Sirlin, C.; Gaiddon, C.; Pfeffer, M. *Dalton Trans.* **2011**, *40*, 8869–78.
- (34) Sohm, F.; Gaiddon, C.; Antoine, M.; Boutillier, A. L.; Loeffler, J. P. *Oncogene* **1999**, *18*, 2762–9.
- (35) Rene, F.; Monnier, D.; Gaiddon, C.; Felix, J. M.; Loeffler, J. P. *Neuroendocrinology* **1996**, *64*, 2–13.
- (36) Gaiddon, C.; Larmet, Y.; Trinh, E.; Boutillier, A. L.; Sommer, B.; Loeffler, J. P. *J. Neurochem.* **1999**, *73*, 1467–76.
- (37) Gaiddon, C.; de Tapia, M.; Loeffler, J. P. *Mol. Endocrinol.* **1999**, *13*, 742–51.
- (38) Gaiddon, C.; Tian, J.; Loeffler, J. P.; Bancroft, C. *Endocrinology* **1996**, *137*, 1286–91.
- (39) Broadley, S. A.; Hartl, F. U. *Trends Cell Biol.* **2008**, *18*, 1–4.
- (40) Puckett, C. A.; Barton, J. K. *Biochemistry* **2008**, *47*, 11711–6.
- (41) Evstatiev, R.; Gasche, C. *Gut* **2012**, *61*, 933–52.
- (42) Kratz, F.; Hartmann, M.; Keppler, B.; Messori, L. *J. Biol. Chem.* **1994**, *269*, 2581–8.
- (43) Fotiadis, D.; Kanai, Y.; Palacin, M. *Mol. Aspects Med.* **2013**, *34*, 139–58.
- (44) Nicklin, P.; Bergman, P.; Zhang, B.; Triantafellow, E.; Wang, H.; Nyfeler, B.; Yang, H.; Hild, M.; Kung, C.; Wilson, C.; Myer, V. E.; MacKeigan, J. P.; Porter, J. A.; Wang, Y. K.; Cantley, L. C.; Finan, P. M.; Murphy, L. O. *Cell* **2009**, *136*, 521–34.
- (45) Groessl, M.; Zava, O.; Dyson, P. J. *Metallomics* **2011**, *3*, 591–9.
- (46) Puckett, C. A.; Ernst, R. J.; Barton, J. K. *Dalton Trans.* **2010**, *39*, 1159–70.
- (47) Romero-Canelon, I.; Pizarro, A. M.; Habtemariam, A.; Sadler, P. J. *Metallomics* **2012**, *4*, 1271–9.